7-6-2005

Electric-field-induced transformation of incommensurate modulations in antiferroelectric Pb0.99Nb0.02[(Zr1−xSnx)1−yTiy]0.98O3

Hui He
Iowa State University

Xiaoli Tan
Iowa State University, xtan@iastate.edu

Electric-field-induced transformation of incommensurate modulations in antiferroelectric Pb0.99Nb0.02[(Zr1−xSnx)1−yTiy]0.98O3

Abstract

Most antiferroelectric ceramics are modified from the prototype $PbZrO_3$ by adding Sn and Ti in conjunction with small amount of Nb or La to optimize their properties. These modifiers introduce unique nanoscale structural feature to the ceramics in the form of incommensurate modulations. It was shown previously that the modulation is strongly responsive to a change in chemical composition or temperature. However, its response to an electric field, the driving force in real applications, has not been explored before. In the present work the dynamic evolution of the incommensurate modulation during the electric field-induced antiferroelectric-to-ferroelectric transformation was observed with an *in situ* transmission electron microscopy (TEM) technique. The results indicate that the incommensurate modulation exists as a transverse Pb-cation displacement wave. The wavelength was found to be quite stable against external electrical stimuli, in sharp contrast to the dramatic change under thermal stimuli reported previously. It is suggested that the appeared incommensurate modulation is an average effect of a mixture of two commensurate modulations. The electric field-induced antiferroelectric-to-ferroelectric transformation proceeds with aligning the Pb-cation displacements, which resembles the process of 90° reorientation and 180° reversal in normal ferroelectrics.

Disciplines

Ceramic Materials | Materials Science and Engineering

Comments

This article is from *Physical Review B* 72 (2005): 024102, doi: 10.1103/PhysRevB.72.024102. Posted with permission.

Electric-field-induced transformation of incommensurate modulations in antiferroelectric $Pb_{0.99}Nb_{0.02}[(Zr_{1-x}Sn_x)_{1-y}Ti_y]_{0.98}O_3$

Hui He and Xiaoli Tan*
Department of Materials Science and Engineering, Iowa State University, Ames, Iowa 50011, USA
(Received 9 February 2005; published 6 July 2005)

Most antiferroelectric ceramics are modified from the prototype $PbZrO_3$ by adding Sn and Ti in conjunction with small amount of Nb or La to optimize their properties. These modifiers introduce unique nanoscale structural feature to the ceramics in the form of incommensurate modulations. It was shown previously that the modulation is strongly responsive to a change in chemical composition or temperature. However, its response to an electric field, the driving force in real applications, has not been explored before. In the present work the dynamic evolution of the incommensurate modulation during the electric field-induced antiferroelectric-to-ferroelectric transformation was observed with an *in situ* transmission electron microscopy (TEM) technique. The results indicate that the incommensurate modulation exists as a transverse Pb-cation displacement wave. The wavelength was found to be quite stable against external electrical stimuli, in sharp contrast to the dramatic change under thermal stimuli reported previously. It is suggested that the appeared incommensurate modulation is an average effect of a mixture of two commensurate modulations. The electric field-induced antiferroelectric-to-ferroelectric transformation proceeds with aligning the Pb-cation displacements, which resembles the process of 90° reorientation and 180° reversal in normal ferroelectrics.

DOI: 10.1103/PhysRevB.72.024102 PACS number(s): 77.80.Bh, 61.44.Fw, 61.14.Lj, 77.80.Dj

I. INTRODUCTION

In many solids a local property, such as electric polarization, magnetization, charge density, mass density, and atomic position, is modulated with a periodicity q_I which is incommensurate to the periodicity q_p of the underlying lattice.[1,2] Such incommensurate modulations have been observed in $PbZrO_3$- and $PbZrO_3$-based ferroelectric and antiferroelectric perovskite, using the selected area electron diffraction (SAED) technique in transmission electron microscopy (TEM).[3–17] Based on the prominent effects of chemical composition and temperature on the modulation wavelength, it has been suggested that frustration from the competing ferroelectric ordering and antiferroelectric ordering is responsible for the presence of the incommensurate structure.[9] However, the exact cause of the incommensurate phase in these oxides is still under debate. Several mechanisms have been offered so far for the structural mechanism, including Pb-cation displacement, O-octahedron tilting, lattice strain, and vacancy ordering.[3–17] One well accepted phenomenon in these polar oxides is that the incommensurate phase would not be observed to develop until the solid is cooled below the Curie temperature, strongly suggesting that the incommensurate structure resides in the polar order. The presence of incommensurate modulations in ferroelectric perovskite is highly unique because cation displacement is coupled with electric polarization in these ceramics.

The $PbZrO_3$-based antiferroelectrics are also of technological importance due to their wide applications in microelectromechanical systems and energy storage devices.[18–21] The electric field-induced antiferroelectric-to-ferroelectric phase transformation forms the physics basis for these applications. However, the transformation requires a so strong electric field in the prototype antiferroelectric $PbZrO_3$ that dielectric breakdown occurs instead.[22,23] Therefore, most antiferroelectric ceramics are chemically modified by adding Sn, Ti, and Nb or La to reduce the critical field and optimize the properties.[3–21] It is widely believed that the reduction in the critical field traces its origins to the hierarchical microstructures: the subgrain level antiferroelectric 90° domains (the checkerboard pattern) and the nanoscale incommensurate modulations within the domains.[4] Presumably the modulation transforms into a commensurate one during the field-induced antiferroelectric-to-ferroelectric phase transformation. However, this has yet to be confirmed experimentally. Furthermore, a structure model for the incommensurate modulation in these oxides is still lacking and the details of the structure of the 90° domain wall in modulated antiferroelectrics have not been revealed so far.[24]

The transformation of the incommensurate modulation in $PbZrO_3$-based antiferroelectrics has been investigated by changing in chemical compositions and temperatures. It is still reasonable to argue that electric field is a much "cleaner," more unidirectional driving force for the incommensurate phase transformation in these electrically active solids. Electric fields are known to enhance ferroelectric ordering and transform antiferroelectric phases into ferroelectric ones.[18–21] On the other hand, electron diffraction, to the authors' best knowledge, is the only technique employed so far to reveal the incommensurate modulation in these ceramics. Therefore, an *in situ* TEM technique capable of delivering high electric fields to TEM specimens while imaging would be ideal for the study of such transformation.[25–27] In the present work, we report detailed information obtained from such *in situ* TEM experiments on the evolution of incommensurate modulations. We then propose a structure model for the incommensurate modulation and the associated antiferroelectric 90° domain walls.

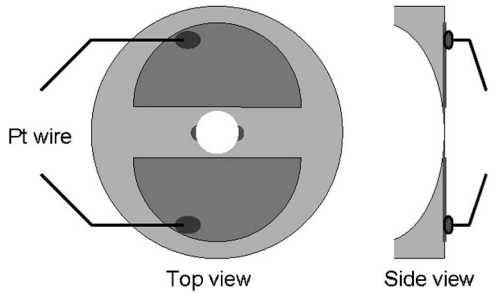

FIG. 1. Schematic diagram of specimens for the electric field *in situ* TEM study. The two dark areas at the edge of the central perforation indicate the area examined in the TEM.

II. EXPERIMENTAL PROCEDURE

Hot pressing after calcination was used to prepare the antiferroelectric ceramic. Raw powders with purity better than 99.9% of PbO, Nb_2O_5, ZrO_2, SnO_2, and TiO_2 were batched according to the chemical formula $Pb_{0.99}Nb_{0.02}[(Zr_{0.58}Sn_{0.42})_{0.955}Ti_{0.045}]_{0.98}O_3$ (abbreviated as PZST 42/4.5/2). Isopropyl alcohol was added to the mixed powders and the slurry was then milled in a plastic bottle with zirconia media on a vibratory mill for 6 h. The slurry was dried in an oven at 150 °C for 24 h. After drying, the powders were calcined at 860 °C for 4 h in a covered alumina crucible. The calcined powder was then milled again for 6 h. After drying, pressed cylinders, 15 mm in diameter by 20 mm high, were formed by cold-isostatic pressing at 350 MPa. The preformed pellets were then hot pressed in an Al_2O_3 die at 1100 °C for 2 h in air. Thin slices from the hot pressed piece were annealed at 1300 °C for 6 h in an atmosphere containing excess PbO. After removal of surface layers by grinding, the annealed slices were polished and electroded. Dielectric characterization was performed with an LCR meter (HP-4284A, Hewlett-Packard) at frequency of 1 kHz in conjunction with an environmental chamber. A heating rate of 3 °C/min was used during measurement. Electric field-induced polarization was recorded with a standardized ferroelectric test system (RT-66A, Radiant Technologies).

After electrical measurements, disks of 3 mm in diameter were ultrasonically cut from the specimens. The thickness of the disks was reduced to about 150 μm by mechanical grinding and polishing. The center portion was further thinned to around 10 μm by mechanical dimpling. Then the specimens were annealed at 250 °C for 30 min to minimize residual stresses. An argon ion mill was used for the final thinning until perforation occurred in the center. Gold electrodes with spacing of 250 μm were evaporated to the TEM specimens and platinum wires were used to connect the electrodes to the electrical contacts on a special double-tilt TEM holder (Gatan, Inc.). Figure 1 shows the schematic diagram of the TEM specimen geometry. Details of the electric field *in situ* TEM technique can be found elsewhere.[25–27] TEM studies were carried out on a Phillips CM-30 microscope operating at 300 kV.

It should be noted that the presence of the central perforation disturbs the electric field between the two half-circle-shaped electrodes. In this study, observations were made on grains located within the two dark areas shown in Fig. 1. For an ideal circular perforation, it was shown that the actual field at these two sites preserves the direction of the nominal field and its magnitude is intensified by a factor of 2.[28] The nominal field equals to the applied voltage divided by the gap spacing. In this article, the value of the electric field strength refers to the actual field at these two sites.

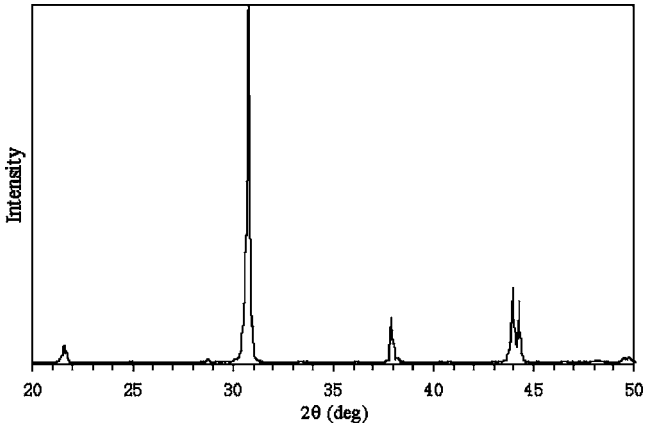

FIG. 2. X-ray diffraction spectrum of the antiferroelectric PZST 42/4.5/2.

III. EXPERIMENTAL RESULTS

A. Average structure and electrical properties

X-ray diffraction was used to determine the average crystal structure of the annealed slices and the spectrum is shown in Fig. 2. The ceramic takes a pseudotetragonal structure with lattice parameters of $a=b=4.116$ Å and $c=4.090$ Å. In this study, we adopt this pseudotetragonal structure for our discussion, even though there is dispute about the fine structure of these ceramics.[13–15,23,24]

Temperature dependence of the dielectric permittivity of PZST 42/4.5/2 is shown in Fig. 3. One distinct feature in the

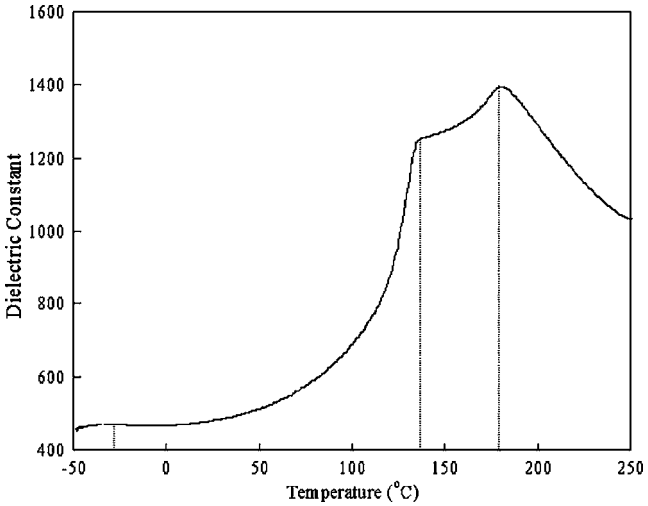

FIG. 3. Temperature dependence of the relative dielectric permittivity at 1 kHz in the PZST 42/4.5/2.

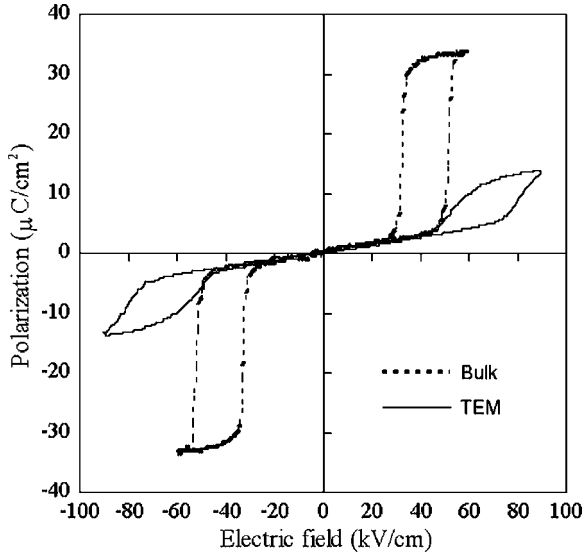

FIG. 4. Electric field-induced polarization measurement at 4 Hz from a bulk circular plate sample and an unperforated TEM specimen.

dielectric response is the existence of a dielectric plateau region between 134 and 180 °C. The dielectric constant peaks with a value of 1394 at the temperature of 180 °C. Two secondary dielectric anomalies are also noticed in this composition. One is at 134 °C and the other is around −34 °C. Based on previous studies on ceramics with similar compositions,[13] the PZST 42/4.5/2 ceramic is paraelectric with cubic structure at temperatures above 180 °C, antiferroelectric with incommensurate modulations between −34 and 134 °C, antiferroelectric with commensurate modulations below −34 °C. The ceramic is in a multicell cubic state in the plateau region from 134 to 180 °C. The multicell cubic region was previously attributed to the disruption of the paraelectric-antiferroelectric transformation by Sn doping.[29]

Electric field-induced antiferroelectric-to-ferroelectric phase transformation is revealed by the polarization measurement. A circular disk specimen with a diameter about 12 mm and a thickness about 300 μm was used. The electric field was applied along the thickness direction at about 4 Hz. The characteristic double hysteresis loops are shown in Fig. 4 with the dashed curve labeled as "bulk." It is evident that the antiferroelectric phase transforms to a ferroelectric phase at a critical electric field about 50 kV/cm (it is referred to as E_F in literature), and the reverse transformation occurs when the field is lowered down to 38 kV/cm (it is referred to as E_A in literature). Both transformations are abrupt and take place within a narrow field strength range.

In order to determine the voltage needed for the *in situ* TEM study and assess the sample geometry effect on the field-induced antiferroelectric-to-ferroelectric phase transformation, a dimpled and annealed 3-mm diameter disc TEM specimen (not perforated) was also tested. This was a TEM specimen prior to the argon ion mill and was electroded in the configuration shown in Fig. 1. Such electrode configuration produces an in-plane electric field between the two half-circle electrodes. The result is plotted in Fig. 4 with the solid line labeled as "TEM." The voltage applied was normalized by the gap spacing 250 μm. Compared to the bulk circular plate sample with electric field along the thickness direction, the TEM-specimen-like disk shows a more gradual phase transformation starting at a higher E_F about 70 kV/cm. The difference in the phase transformation behavior of the two types of specimen may arise from the different geometries, including the electrode geometry and the thickness difference. For the TEM-specimen-like disk, the field was applied to a thickness-varying portion, with the thinnest part around 10 μm, comparable to the grain diameter in the material.

B. The incommensurate modulation

Conventional TEM examination reveals that the antiferroelectric PZST 42/4.5/2 ceramic displays hierarchical microstructural features, as shown in Fig. 5. The characteristic checkerboard patterns of antiferroelectric 90° domains were found in the majority of the grains, as shown in Fig. 5(a) where the electron beam was along the [001] direction. The 90° domain walls roughly follow the (100) or (010) plane. Small segments were also found to be parallel to the {110} plane.

Close up examination of individual 90° domains along [001] zone axis reveals the incommensurate modulation stripes along {110} planes and selected area diffraction shows the corresponding satellite spots surrounding fundamental reflections [Fig. 5(b)]. In general, the satellite reflections in these modified antiferroelectric ceramics can be expressed as $ha^*+kb^*+lc^*\pm(1/n)\{a^*+b^*\}$, where h, k, l are integers and n can be directly measured from the diffraction pattern. The measured n can be used to derive the modulation wavelength if lattice parameters are known. From the inset of Fig. 5(b), n is measured to be 6.02, which gives a wavelength of 1.75 nm. This value matches exactly to the direct measurement from the image. Close examination of the electron diffraction pattern shows that all the satellite spots around the hh0-type fundamental spots (these fundamentals are sitting on the row including the transmitted spot) are much weaker than the others. According to Zuo and Tao's analysis on a different perovskite oxide,[30] this suggests that the incommensurate modulation exists in the form of a transverse atomic displacement wave. Therefore, our study supports the Pb-cation displacement structural mechanism.

When the selected area includes a 90° domain wall, two sets of satellite spots are obtained, as depicted in Fig. 5(c). Careful measurements from the inset diffraction pattern indicate that $n=6.97$ for the vertical set of satellite spots (the corresponding modulation stripes in the image are in the horizontal direction with a wavelength of 2.03 nm) while $n=7.33$ for the horizontal set of satellite spots (the corresponding modulation stripes in the image are in the vertical direction with a wavelength of 2.13 nm). It is evident, therefore, that the modulation wavelength varies even across a 90° domain wall within a single grain. It should be noted that the material was annealed at 1300 °C for 6 h after hot pressing. Therefore, the difference was likely to be caused by residual stresses, not by heterogeneity in chemical composition. It is also interesting to note that the 90° domain wall in Fig. 5(c)

deviated from the (100) plane. This will be addressed in detail in the discussion section in the following. Again, the weaker satellite spots in the vertical set in the column passing through the transmitted beam and those in the horizontal set in the row passing through the transmitted beam than the others suggest a primary contribution from the Pb-cation displacements.

C. *In situ* TEM study

In situ TEM studies were carried out on a specimen that was crack free at the edge of the central perforation. For an ideal circular-shaped perforation, the actual electric field at the two sites that are highlighted in Fig. 1 is intensified by a factor of 2 (Ref. 28). The direction of the actual field at these two sites preserves the direction of the undisturbed field which is perpendicular to the electrode edges. When this specimen was loaded to the special TEM holder, the gap between the two half-circle electrodes was aligned with the long axis of the whole holder, in other words, the primary tilting axis. In such a configuration, the undisturbed electric field (the nominal electric field) is along the secondary tilting axis, perpendicular to the primary tilting axis. Based on this relation, the direction of the actual electric field is determined.

Electron transparent grains within the two highlighted areas outlined in Fig. 1 in the specimen were examined in the TEM. One of the grains was found to have its [001] axis parallel to the electron beam without secondary tilting. This grain was about 5 μm in size. The [001] zone-axis SAED pattern was recorded at different field levels to monitor the evolution of the incommensurate modulation. The electric field strength was estimated by doubling the nominal field strength.

The change of the satellite spots in the [001] zone-axis SAED pattern under static electric field is depicted in Fig. 6. Initially, this grain displays two sets of satellite reflections. As evident in Fig. 6(a), the satellite spots are strong in intensity and slightly elongated in shape. Similar to the diffraction pattern shown in the inset of Fig. 5(c), the difference in the intensity of satellite spots was again observed, indicating a transverse Pb-cation displacement wave. Next, static electric fields were applied and increased stepwise. The applied field direction was determined to be along the gray line in Fig. 6(b). At an actual electric field of 60 kV/cm, the horizontal set of satellite spots almost completely disappeared. For the vertical set, many satellite spots disappeared as well and the remaining spots exhibited severe streaking [Fig. 6(b)].

The bright rectangular boxes in Figs. 6(a) and 6(b) enclose two fundamental reflections of 120 and 210. The appearance of the satellite spots of these two fundamental reflections at a series of field levels of 0, 8, 20, 30, 40, and 60 kV/cm is shown in Fig. 7. It is evident that satellite reflections in both sets started to become weaker at an electric field of 8 kV/cm, which is far below the macroscopic critical field for the antiferroelectric-to-ferroelectric phase transformation. The satellite spots in the horizontal set almost completely disappeared at 40 kV/cm and became slightly diffused before their final disappearance. On the other hand, the satellite reflections in the vertical set started to show severe streaking at 20 kV/cm and their presence persists up to 60 kV/cm. This shows an orientation dependence of their response to the external field. Details will be discussed in the next section.

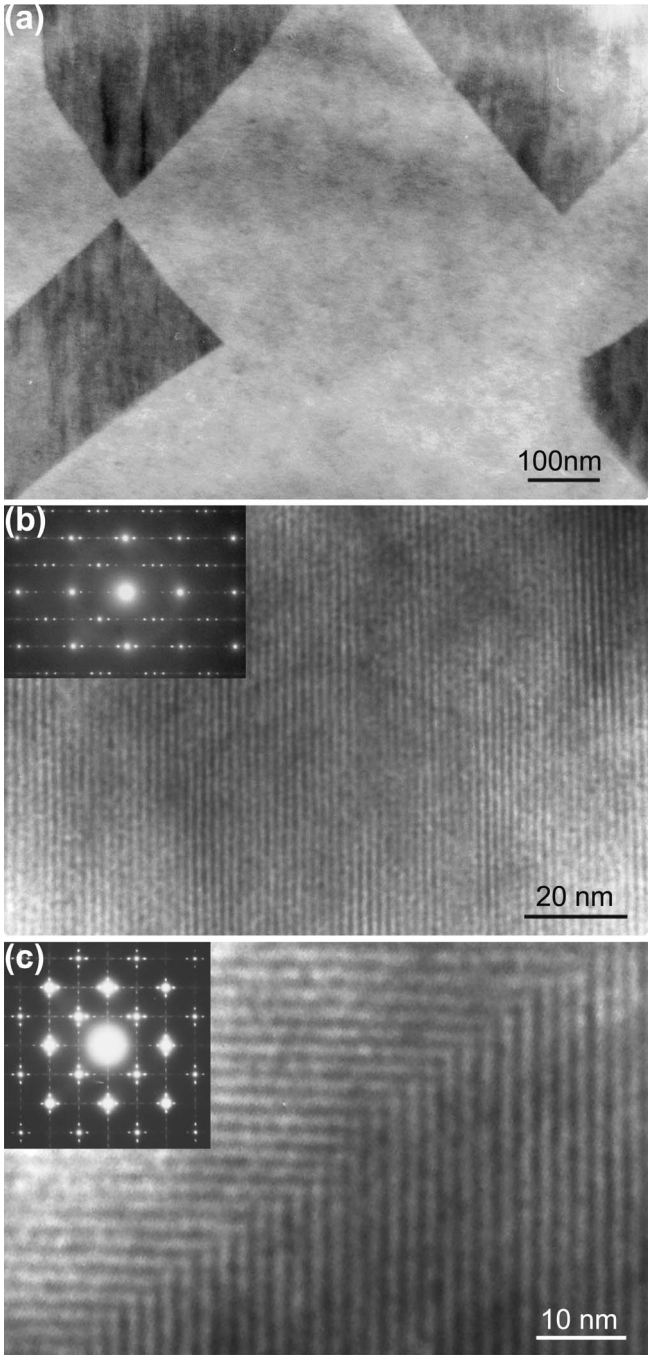

FIG. 5. The hierarchical structure in the antiferroelectric PZST 42/4.5/2. (a) The checkerboard pattern of antiferroelectric 90° domains, (b) the incommensurate modulation in one domain, and (c) the incommensurate modulation across the 90° domain wall.

The value of n in $ha^*+kb^*+lc^*\pm(1/n)\{a^*+b^*\}$ was measured from electron diffraction patterns at different field levels and is plotted in Fig. 8. At each field level, at least ten pairs of satellites were measured. For diffused satellite spots, the measurement was performed at the point with the highest

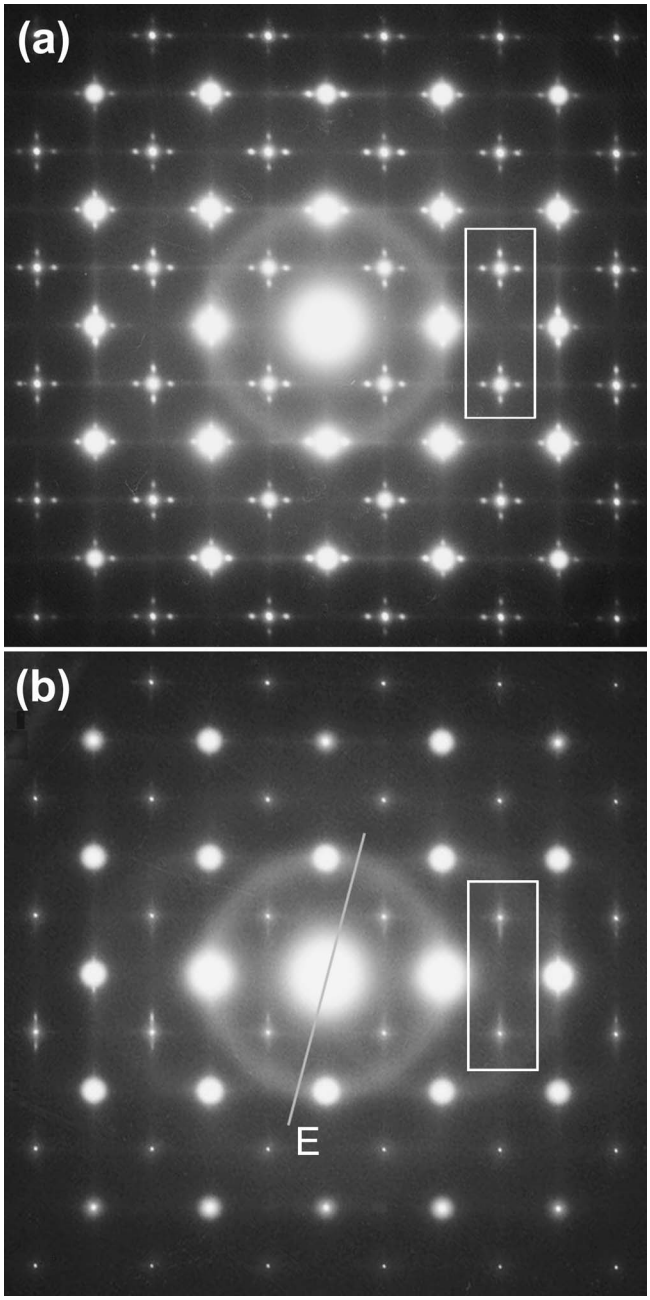

FIG. 6. Change of the satellite reflections in the ⟨001⟩ zone axis selected area diffraction pattern under external electric field. (a) $E=0$ and (b) $E=60$ kV/cm. The gray line indicates the direction of the applied field. The two rectangular boxes enclose the 120 and 210 fundamental reflections.

intensity. Again, a significant difference in n occurred across a 90° domain wall within a single grain. At zero field, $n=6.78$ for the horizontal set of satellite spots, corresponding to a wavelength of 1.97 nm, and $n=7.67$ for the vertical, corresponding to 2.23 nm. It should be noted that the grain was about 5 μm in size and the material was annealed at 1300 °C for 6 h after hot pressing. Therefore, residual stresses are likely to be responsible for the significant difference in wavelength.

Another evident feature in Fig. 8 is the negligible change in the incommensurate modulation wavelength under strong

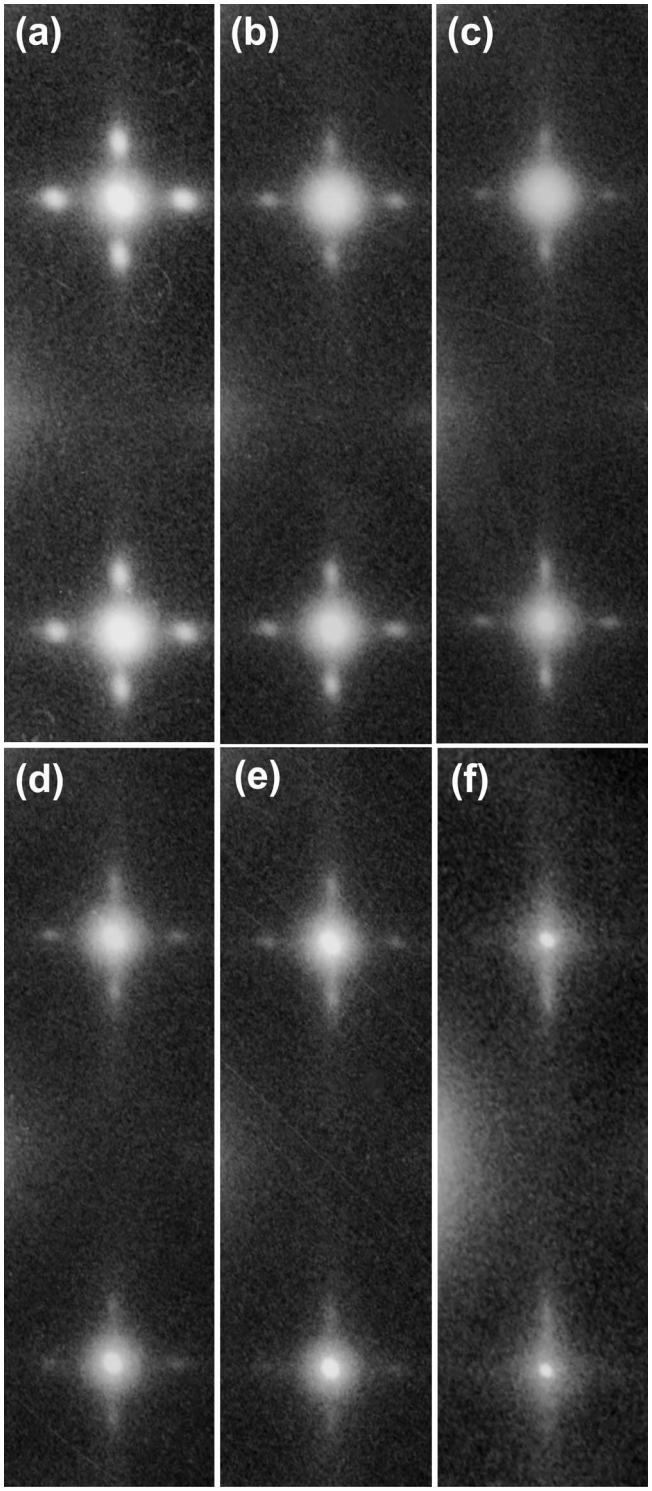

FIG. 7. Evolution of the satellite reflections surrounding the 120 and 210 fundamental reflections. (a) $E=0$, (b) $E=8$ kV/cm, (c) $E=20$ kV/cm, (d) $E=30$ kV/cm, (e) $E=40$ kV/cm, and (f) $E=60$ kV/cm.

applied electric fields. A linear fit to the mean value of n gives a slope of −0.0061 Å per kV/cm for the horizontal set and −0.0035 Å per kV/cm for the vertical set, respectively. The higher rate of change for the horizontal set is in accordance with the evolution of the satellite spots of that set

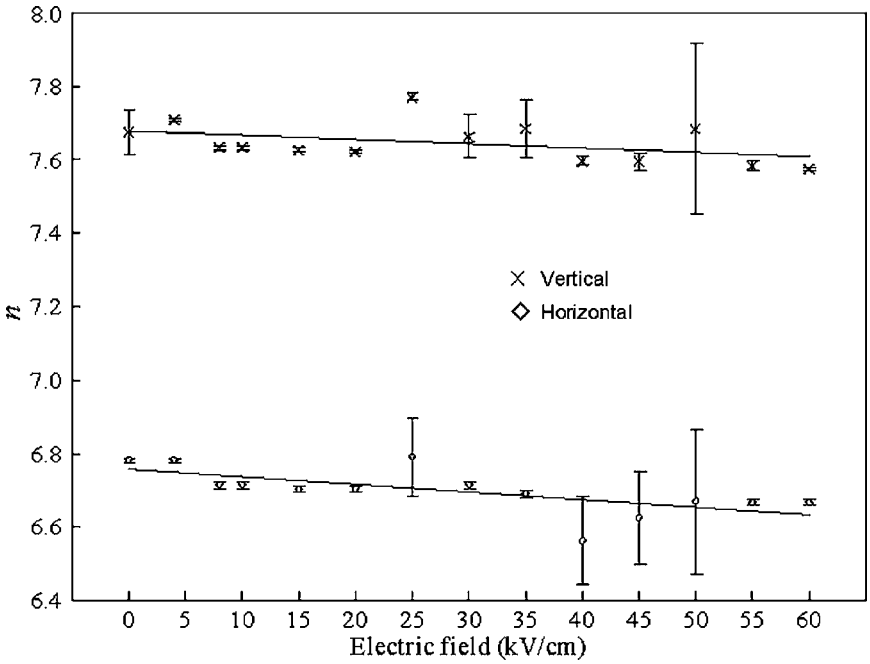

FIG. 8. Change of n value with applied electric fields for the vertical set and horizontal set of satellite reflections shown in Figs. 6 and 7.

under electric fields. It was shown in Fig. 7 that these spots disappeared at a lower field level. The wavelength in real space decreases slightly with increasing electric fields for both sets. At 40 kV/cm, it was recorded as 1.95 nm (a 1.2% decrease from the initial wavelength) for the horizontal set and 2.22 nm (a 0.7% decrease from the initial wavelength) for the vertical set, respectively.

IV. DISCUSSION

Although incommensurate modulations in perovskite antiferroelectrics modified from $PbZrO_3$ were first observed twenty years ago,[3] there have been very limited publications on this issue. A structural model for the modulation wave is still missing. Based on previous studies and the results obtained in this study, we propose a model for the observed incommensurate modulation in these perovskite antiferroelectrics. The model sheds light on the detailed structure of the antiferroelectric 90° domain wall and explains the orientation dependence of the response to applied electric field.

It has been well established that the Pb-cation in the parent $PbZrO_3$ structure is displaced with a periodicity of four layers of its pseudotetragonal {110} plane.[22,23] The SAED patterns shown in Figs. 5 and 6 indicate that the satellite reflections are also originated primarily from transverse Pb-cation displacement modulation waves in the modified antiferroelectrics. We believe that the structure of the commensurate modulation in the parent $PbZrO_3$ can be extended to the observed incommensurate modulations. The observed incommensurate modulation is an average effect over an ensemble of stripes of commensurate modulations. This is illustrated schematically in Fig. 9. Figure 9(a) redraws the structural model of $PbZrO_3$ proposed by Sawaguchi *et al.*,[22] where stripes of the commensurate modulation of Pb-cation displacements with periodicity of four pseudotetragonal {110} planes are evident. Figure 9(b) schematically depicts that an incommensurate modulation can be composed of commensurate modulations. In this illustration, the periodicity of the incommensurate modulation lies somewhere between seven and eight pseudotetragonal {110} planes. Such an incommensurate modulation is composed of stripes of periodicities of $n=7$ and 8, which are commensurate to the underlying lattice. In the SAED pattern, the satellite reflections appear to be incommensurate due to an average effect.

This structure model gains support from the following evidences. The first evidence is related to the change of the incommensurate modulation when chemical composition or temperature varies. In the series of antiferroelectric $Pb_{0.99}Nb_{0.02}[(Zr_{0.55}Sn_{0.45})_{1-y}Ti_y]_{0.98}O_3$ $(y=0.00,0.03,0.06)$, incommensurate satellite reflections are observed in compositions with $y=0.06$ and 0.03. When y is further reduced to zero, where the composition becomes $Pb_{0.99}Nb_{0.02}(Zr_{0.55}Sn_{0.45})_{0.98}O_3$, the incommensurate satellite reflections transform into commensurate ones that are isomorphous to the parent $PbZrO_3$ (Ref. 13). It was also found in this series (the $Pb_{0.99}Nb_{0.02}[(Zr_{0.58}Sn_{0.42})_{0.96}Ti_{0.04}]_{0.98}O_3$ composition) that the room-temperature antiferroelectric phase with incommensurate modulations transforms to an antiferroelectric one with a structure isomorphous to $PbZrO_3$ when cooled down below −150 °C (Ref. 15). Furthermore, the parent $PbZrO_3$ itself was observed to display incommensurate satellite reflections when heated up to a narrow temperature range between 225 and 230 °C (Ref. 14). These findings from previous studies reveal strong and direct connections between the appeared incommensurate modulations and the commensurate modulations in these ceramics. Therefore, the structure of the observed incommensurate modulations should bear intrinsic similarities to the structure of the parent $PbZrO_3$.

The second evidence arises from a survey on the n value reported in literature. The result is summarized in Table I with references, including both the $PbZrO_3$ and the modified antiferroelectric ceramics. Commensurate modulations do

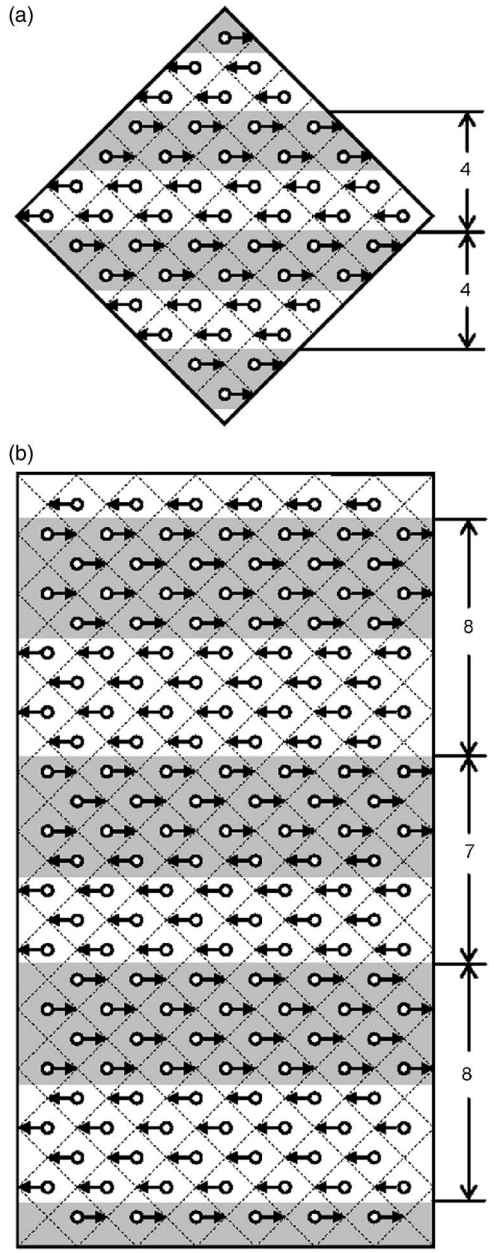

FIG. 9. Structure models for perovskite antiferroelectrics. (a) The structure proposed by Sawaguchi *et al.* (Ref. 22) for $PbZrO_3$, (b) the structure of the modulation in this study. The incommensurate modulation is suggested to be a mixture of commensurate modulations.

appear in these ceramics. For example, $n=7$ and $n=8$ were reported in the $Pb_{0.99}Nb_{0.02}[(Zr_{0.80}Sn_{0.20})_{0.97}Ti_{0.03}]_{0.98}O_3$ in Ref. 3. It is interesting to notice that, for those non-integer n values, simple combinations of two neighboring integers can be always found to generate the noninteger n when averaged. These combinations are listed in the fourth column of Table I. It is proposed that the incommensurate modulation in $PbZrO_3$ at 225 °C with $n=6.67$ can be comprised of stripes of commensurate modulations with $n=6$ and $n=7$. When one stripe modulated with $n=6$ appears after every two stripes with $n=7$, an overall $n=6.67$ would be seen over a large volume. For the PZST 42/4.5/2 oxide examined in this study, five different n values are measured from electron diffraction patterns recorded in different areas. For the values of 6.02 and 6.97, we believe they are modulated commensurately with $n=6$ and $n=7$, respectively. The modulation with $n=6.78$ can be considered as a mixture of commensurate modulations of $n=6$ and $n=7$ with a repeating pattern of 7/6/7/7; the 7.33 as a mixture with a pattern of 7/8/7; and the 7.67 as one with a pattern of 8/7/8. Under the conditions of the selected area electron diffraction, an area within a 90° domain is used to produce the diffraction pattern. This area is typically on the order of 1 μm, therefore, containing several hundreds of modulation stripes. The observed satellite reflections then show an average wavelength over the selected area (volume).

In a recent study on the antiferroelectric $Pb_{0.97}La_{0.03}(Zr_{0.95}Ti_{0.05})O_3$, Asada and Koyama[17] observed discrete n values when the oxide was heated from room temperature. This is the third evidence supporting our model. Below 73 °C, n was measured to be 4.0. From 73 to 122 °C, $n=6.0$ was recorded. From 122 to 160 °C, $n=6.5$; from 160 to 180 °C, $n=7.0$; while above 180 °C, $n=7.5$. These authors hence claimed that the material is commensurately modulated. We suggest that the modulations at different temperatures are not only commensurate, but also have an integer number of layers of the pseudotetragonal {110} planes within a period. The modulation with overall $n=6.5$ is thus a mixture of modulations with local $n=6$ and $n=7$ while the one with overall $n=7.5$ is mixture of that with local $n=7$ and $n=8$.

The most direct evidence may be due to Cai *et al.*[16] These researchers measured $n=7.24$ from the SAED pattern in antiferroelectric $Pb_{0.97}La_{0.02}(Zr_{0.66}Sn_{0.25}Ti_{0.09})O_3$. According to our model, the appeared incommensurate modulation is comprised of commensurately modulated stripes with a pattern of 7/7/8/7 on statistical average. And indeed, they observed stripes with commensurate modulations. The high-resolution lattice image revealed a sequence of $\cdots$7/7/7/7/7/8/7/7/8/7/7/7/8/7$\cdots$.

These evidences support the model described in Fig. 9. The observed incommensurate modulation is actually a mixture of commensurate modulations. The modulation exists in the form of a transverse Pb-cation displacement wave. However, the magnitude of the displacement is a constant and the wave is not a sinusoidal wave. This model thus bears intrinsic similarities to the antiferroelectric structure of $PbZrO_3$. The model also sheds light on the fact that higher order satellite reflections are often observed when the satellites are commensurate while only the first order satellites are observed when the satellites are incommensurate. The incommensurate satellites are generated by a mixture of two commensurate modulations. Thus, the appeared incommensurate modulation exhibits less degree of order.

The structure model implies that the modulation within a 90° domain is a stack of 180° domains with antiparallel Pb-cation displacement. For most antiferroelectric ceramics, the component commensurate modulations for the observed incommensurate modulations have $n=6$, 7, and 8, as demonstrated in Table I. Therefore, the 180° domains in these antiferroelectrics have a thickness of three or four layers of the pseudotetragonal {110} plane. For the parent $PbZrO_3$, the 180° domains are two layers of {110} plane thick. These 180°

TABLE I. Reported n in various antiferroelectric ceramics.

Compositions	Temp.	n	Commensurate stripes	Ref.
$PbZrO_3$	225 °C	6.67	7/6/7	14
$Pb_{0.97}La_{0.03}(Zr_{0.95}Ti_{0.05})O_3$	25 °C	4.00		17
	73 °C	6.00		
	122 °C	6.50	6/7	
	160 °C	7.00		
	180 °C	7.50	7/8	
$Pb_{0.97}La_{0.02}(Zr_{0.66}Sn_{0.25}Ti_{0.09})O_3$	25 °C	7.24	7/7/8/7	16
$Pb_{0.97}La_{0.02}(Zr_{0.65}Sn_{0.25}Ti_{0.10})O_3$	25 °C	9.00		4
$Pb_{0.99}Nb_{0.02}(Zr_{0.55}Sn_{0.45})O_3$	25 °C	4.00		13
$Pb_{0.99}Nb_{0.02}[(Zr_{0.55}Sn_{0.45})_{0.97}Ti_{0.03}]O_3$	25 °C	6.73	7/7/6/7	
$Pb_{0.99}Nb_{0.02}[(Zr_{0.55}Sn_{0.45})_{0.94}Ti_{0.06}]O_3$	25 °C	8.00		
$Pb_{0.99}Nb_{0.02}[(Zr_{0.58}Sn_{0.42})_{0.96}Ti_{0.04}]O_3$	25 °C	7.00		15
		6.67	7/6/7	
$Pb_{0.99}Nb_{0.02}[(Zr_{0.80}Sn_{0.20})_{0.97}Ti_{0.03}]O_3$	25 °C	7.00		3
		8.00		
$Pb_{0.99}Nb_{0.02}[(Zr_{0.80}Sn_{0.20})_{0.97}Ti_{0.03}]O_3$	25 °C	7.49	7/8	10
$Pb_{0.99}Nb_{0.02}[(Zr_{0.70}Sn_{0.30})_{0.97}Ti_{0.03}]O_3$	25 °C	7.51	7/8	
$Pb_{0.99}Nb_{0.02}[(Zr_{0.60}Sn_{0.40})_{0.97}Ti_{0.03}]O_3$	25 °C	6.76	7/6/7/7	
$Pb_{0.99}Nb_{0.02}[(Zr_{0.50}Sn_{0.50})_{0.97}Ti_{0.03}]O_3$	25 °C	6.68	7/6/7	
$Pb_{0.99}Nb_{0.02}[(Zr_{0.58}Sn_{0.42})_{0.955}Ti_{0.045}]O_3$	25 °C	6.02	6	This study
		6.78	7/6/7/7	
		6.97	7	
		7.33	7/8/7	
		7.67	8/7/8	

domains are shaded differently in Fig. 9 for clarity.

When the modulation wavelength is the same on both sides of a 90° domain wall, the Pb-cation displacement can be easily arranged to a "head-to-tail" configuration in order to achieve charge neutrality at the 90° domain wall.[24] However, it is noticed in Fig. 5(c) and Fig. 8 that the modulation wavelength changes significantly across a 90° domain wall. This may lead to a situation that a 180° domain of three layers {110} plane thick meets one of four layers thick at the 90° domain wall. It can be shown that the charge neutrality is still preserved when an atomic step is created on the 90° domain wall. Figure 10 schematically illustrates such a situation. The upper-right 90° domain bears a modulation with $n=8$ (the 180° domain slabs in this 90° domain have a thickness of four layers of the {110} plane) while the lower-left domain bears one with $n=7$ (the 180° domain slabs in this 90° domain have a thickness of three or four layers of the {110} plane). The 180° domain slabs are highlighted with different shades. It shows clearly that the atomic step on the 90° domain wall mediates the difference in wavelength and preserves the "head-to-tail" configuration. Such a mechanism implies that the 90° domain wall would follow the {100} plane if the two 90° domains have identical modulation wavelength and would deviate from the {100} plane if the two domains have different wavelengths. This is indeed the case. In $PbZrO_3$, all the modulations have identical wavelength and the 90° domain wall was observed to be parallel to the {100} plane.[24] In the PZST 42/4.5/2 investigated in this study, it is shown in Fig. 5 that the 90° domain wall is tilted away from the {100} plane due to the difference in the modulation wavelength.

With the proposed structure models for the incommensurate modulation and the 90° domain wall, we now can picture the evolution of the modulations during the electric field-induced antiferroelectric-to-ferroelectric phase transformation. A fundamental difference in the response of the modulation wavelength to external electric fields is noticed in our study: the wavelength is quite stable against electric stimuli. In the PZST 42/4.5/2 studied here, about 1% decrease in wavelength was measured when an electric field of 40 kV/cm was applied. In contrast to this, Asada and Koyama[17] observed a 88% increase in wavelength when the antiferroelectric $Pb_{0.97}La_{0.03}(Zr_{0.95}Ti_{0.05})O_3$ was heated from room temperature to 180 °C. Xu *et al.*[15] measured a 40%

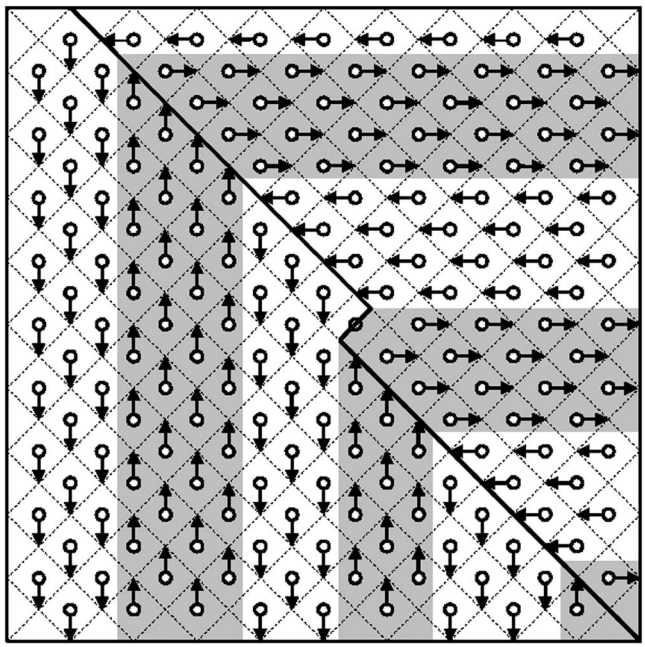

FIG. 10. The structure of the 90° domain wall in $PbZrO_3$-based antiferroelectrics with incommensurate modulations. When the modulation wavelength is not equal on the two sides of the domain wall, atomic steps are introduced to preserve charge neutrality.

increase in wavelength in a composition very close to ours when temperature was increased from 25 to 150 °C. We thus speculate that the electric field-induced antiferroelectric-to-ferroelectric phase transformation starts with a process of aligning the Pb-cation displacements. The aligning process may be initiated preferentially from sites such as grain boundaries and 90° domain walls at a field as low as 8 kV/cm. The volume with aligned cation displacement no longer contributes to the satellite reflections and fraction of the volume increases with increasing electric field. Therefore, the intensity of the satellite reflections starts to decrease at 8 kV/cm, as revealed in Fig. 7.

The aligning process of Pb-cation displacement also explains the orientation dependence of the satellites response revealed in Figs. 6 and 7. When the electric field direction shown in Fig. 6 is translated into Fig. 10, the applied field is seen to be 15° away from the Pb-cation displacement vectors in the lower-left 90° domain (this domain generates the horizontal set of satellite reflections) and 75° away from the displacement vectors in the upper-right 90° domain (this domain generates the vertical set of satellite reflections). Along the direction of Pb-cation displacement, the lower-left 90° domain would experience a resolved field of $0.96E$ while the upper-right one would experience a resolved field of only 0.26E, where E is the amplitude of the applied field. This can be stated in another way, the aligning process of Pb-cation displacement involves a 180°-domain-switching-like process in the lower-left domain and a 90°-domain-switching-like process in the upper-right one. It is well known that in perovskite normal ferroelectrics, 90° domain switching is always more difficult than 180° domain switching. This explains the orientation dependence of the response of the satellites to external electric fields very well. In Figs. 6 and 7, the horizontal set of satellite spots disappeared at a lower level of electric field and showed little streaking before their final disappearance. In the 90° domain that contributes to this set of satellites, the aligning of the Pb cation is more like a 180° domain switching in normal ferroelectrics. Since the 180° domain slabs are very thin, three or four layers of the {110} plane in most cases, switching may well take place at once for the whole thickness. This would decrease the intensity of the corresponding satellites but preserves the wavelength. In contrast, the vertical set of satellite reflections in Figs. 6 and 7 persists to a higher electric field. The aligning process of Pb-cation displacement in the corresponding antiferroelectric 90° domain resembles the 90°-domain-switching process in a normal ferroelectrics. Furthermore, such a 90° reorientation may well disrupt the modulation, leading to a severe streaking in the satellite reflections.

V. CONCLUSIONS

Our TEM study indicates that the incommensurate modulation in modified perovskite antiferroelectrics exists in the form of a transverse Pb-cation displacement wave. The observed incommensurate modulation at large scale is suggested to be a mixture of commensurate modulations at local scale. The modulations in antiferroelectric 90° domains are then 180° domain slabs with thickness of three or four layers of the pseudotetragonal {110} plane. The antiferroelectric 90° domain wall deviates from the pseudotetragonal {100} plane due to the atomic steps on the domain wall created to preserve charge neutrality.

The external electric field aligns the cation displacement prior to the field-induced antiferroelectric-to-ferroelectric phase transformation. The fraction of the volume with aligned cation displacement increases with increasing electric fields, which leads to a decrease in the intensity of the corresponding satellite reflections in the selected area electron diffraction patterns. The cation displacement aligning process resembles the 90° and 180° domain switching process in normal ferroelectrics. When the field is applied along the cation displacement direction, the aligning process is easier and the process preserves, to some extent, the wavelength. The modulation is disrupted when the field is applied perpendicular to the direction of cation displacement and severe streaking is observed in the corresponding satellite reflections.

ACKNOWLEDGMENTS

This work was supported by the National Science Foundation through the CAREER Grant No. DMR-0346819. The experimental work was carried out at the Center for Microanalysis of Materials, University of Illinois at Urbana and Champaign and at the Materials & Engineering Physics Program, Ames Laboratory, U.S. DOE.

*Electronic address: xtan@iastate.edu

[1] http://www.mapr.ucl.ac.be/~crystal/
[2] http://www.cryst.ehu.es/icsdb/index.html
[3] Y. Chang, J. Lian, and Y. Wang, Appl. Phys. A: Solids Surf. **36**, 221 (1985).
[4] J. S. Speck, M. De Graef, A. P. Wilkinson, A. K. Cheetham, and D. R. Clarke, J. Appl. Phys. **73**, 7261 (1993).
[5] Z. Xu, D. Viehland, P. Yang, and D. A. Payne, J. Appl. Phys. **74**, 3406 (1993).
[6] Z. Xu, X. Dai, and D. Viehland, Phys. Rev. B **51**, 6261 (1995).
[7] X. Dai, Z. Xu, J. Li, and D. Viehland, J. Mater. Res. **11**, 626 (1996).
[8] J. Ricote, D. L. Corker, R. W. Whatmore, S. A. Impey, A. M. Glazer, J. Dec, and K. Roleder, J. Phys.: Condens. Matter **10**, 1767 (1998).
[9] D. Viehland, X. H. Dai, J. F. Li, and Z. Xu, J. Appl. Phys. **84**, 458 (1998).
[10] D. Forst, J. F. Li, Z. Xu, and D. Viehland, J. Am. Ceram. Soc. **81**, 2225 (1998).
[11] S. Watanabe and Y. Koyama, Phys. Rev. B **66**, 134102 (2002).
[12] J. Knudsen, D. I. Woodward, and I. Reaney, J. Mater. Res. **18**, 262 (2003).
[13] D. Viehland, D. Forst, Z. Xu, and J. F. Li, J. Am. Ceram. Soc. **78**, 2101 (1995).
[14] Z. Xu, X. Dai, D. Viehland, and D. A. Payne, J. Am. Ceram. Soc. **78**, 2220 (1995).
[15] Z. Xu, D. Viehland, and D. A. Payne, J. Mater. Res. **10**, 453 (1995).
[16] Y. Gai, F. Phillipp, A. Zimmermann, L. Zhou, F. Aldinger, and M. Ruhle, Acta Mater. **51**, 6429 (2003).
[17] T. Asada and Y. Koyama, Phys. Rev. B **69**, 104108 (2004).
[18] B. Jaffe, W. R. Cook, and H. Jaffe, *Piezoelectric Ceramics* (Academic, London, 1971).
[19] K. Uchino, Jpn. J. Appl. Phys., Part 1 **24**, 460 (1985).
[20] W. Pan, Q. Zhang, A. Bhalla, and L. E. Cross, J. Am. Ceram. Soc. **72**, 571 (1989).
[21] B. Xu, L. E. Cross, and J. J. Bernstein, Thin Solid Films **377-378**, 712 (2000).
[22] E. Sawaguchi, H. Maniwa, and S. Hoshino, Phys. Rev. **83**, 1078 (1951).
[23] F. Jona, G. Shirane, F. Mazzi, and R. Pepinsky, Phys. Rev. **105**, 849 (1957).
[24] M. Tanaka, R. Saito, and K. Tsuzuki, Jpn. J. Appl. Phys., Part 1 **21**, 291 (1982).
[25] X. Tan, Z. Xu, J. K. Shang, and P. Han, Appl. Phys. Lett. **77**, 1529 (2000).
[26] X. Tan and J. K. Shang, Philos. Mag. A **82**, 1463 (2002).
[27] H. He and X. Tan, Appl. Phys. Lett. **85**, 3187 (2004).
[28] R. M. McMeeking, ZAMP **40**, 615 (1989).
[29] D. Viehland, D. Forst, and J. Li, J. Appl. Phys. **75**, 4137 (1994).
[30] J. M. Zuo and J. Tao, Phys. Rev. B **63**, 060407 (2001).